

Research Papers

Cooling performance optimization of air cooling lithium-ion battery thermal management system based on multiple secondary outlets and baffle



Furen Zhang^{*}, Peiwen Liu, Yanxiao He, Shiyuan Li

School of Mechatronics & Vehicle Engineering, Chongqing Jiaotong University, Chongqing 400074, China

ARTICLE INFO

Keywords:

Battery thermal management
Air cooling
CFD
Secondary outlet
Baffle

ABSTRACT

Air cooling has attracted extensive attention in the field of battery thermal management (BTMS). A comprehensive optimization scheme adding secondary outlets and baffle was proposed in this paper to improve the cooling performance of the BTMS. Computational fluid dynamics (CFD) was conducted to investigate the influences of the number and width of secondary outlets and baffles on the cooling performance of the BTMS. The effectiveness of CFD method was verified by the air cooling heat dissipation experiment of battery pack. Firstly, the effects of the number and width of the secondary outlets were discussed and optimized. The results showed that, comparing with the initial Z-type BTMS, the maximum temperature (T_{max}) and the maximum temperature difference (ΔT_{max}) were reduced by 1.84 °C (4.20%) and 3.66 °C (75%) after optimization, respectively. Then, based on the above optimization model, a baffle had been added in the cooling channel to further better the air volume distribution and enhance the cooling performance. Compared with the initial Z-type BTMS, T_{max} of the optimum model was reduced by 2.17 °C (4.95%) and ΔT_{max} was reduced by 4.49 °C (91.89%). It can be seen that the optimization method proposed in this paper could be used to design the BTMS for electric vehicle.

1. Introduction

With the development of science and technology, environmental pollution and energy shortage have attracted great attention all over the world. While fuel vehicles are not only one of the major pollution sources, but also one of the major fuel consumables. To solve this problem, automobile manufactures and researchers try to use environment-friendly electric vehicles to replace fuel vehicles. Battery package is one of the most critical components of electric vehicle, and the performance of which determines the mileage and safety of electric vehicle to a great extent. At present, the battery can be divided into lead-acid battery, lithium-ion battery, Ni MH battery and so on. Lithium-ion battery is widely loved by people for its high energy density, no memory, multiple cycles, long life, high efficiency and environmental friendliness [1].

Previous studies have found that the battery can work normally when its temperature is between 20 and 45 °C [2], while for power batteries, the maximal temperature difference between batteries should be less than 5 °C [3]. However, in the process of battery operation, the chemical reaction inside the battery will produce a lot of Joule heat. If there is no effective cooling device, with the increase of heat, the battery

temperature will rise sharply. If battery temperature exceeds the acceptable range of the battery, it will lead to the damage and failure of the battery pack, and even serious safety accidents. In order to make the battery work in a normal state, a reliable thermal management system to cool the battery is essential [4].

Nowadays, there are a variety of cooling methods for batteries, including, air cooling [5–7], liquid cooling [8–11], phase change material cooling [12–15] and heat pipe cooling [16–18]. Among them, with the advantages of simple structure, low cost, no leakage and no extra weight, air cooling has become an easy way to achieve [19]. To date, a large number of scholars have done a lot of research on air-cooling BTMS and have obtained many informative results by different methods.

Ventilation way is the first factor to be considered in air cooling. Pesaran et al. [20] analyzed the cooling performance of series ventilation and parallel ventilation through finite element method. The results showed that T_{max} and ΔT_{max} of the parallel ventilation model were reduced by 4 °C and 10 °C, respectively, compared with the series ventilation model. It indicates that the cooling performance of the parallel air cooling system is higher than that of the series air cooling system. Through introducing the reverse stratified air flow into BTMS, Na et al. [21] reduced T_{max} and ΔT_{max} of the system by 0.6 °C and 13.5%,

* Corresponding author.

E-mail address: zfr@cqjtu.edu.cn (F. Zhang).

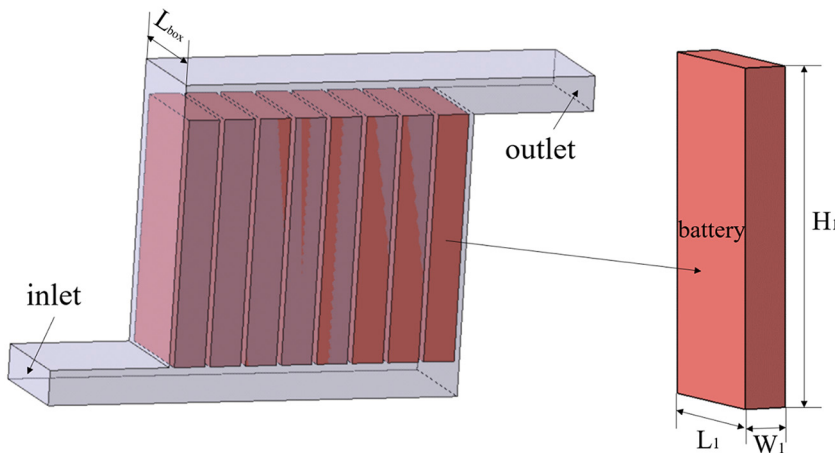


Fig. 1. Schematic of the three-dimensional parallel air-cooled BTMS.

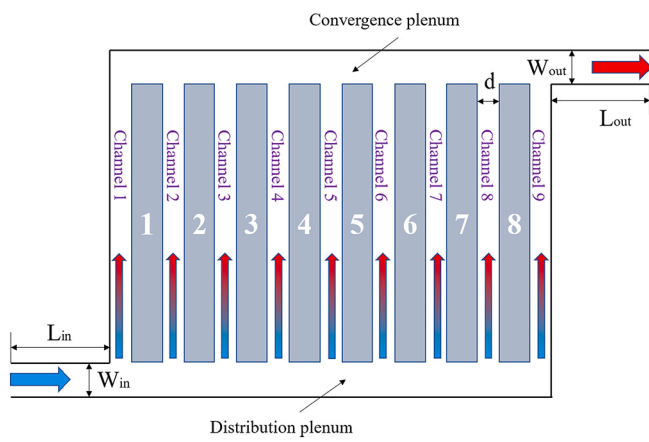


Fig. 2. Dimension parameter of the parallel air-cooled BTMS.

Table 1
Lithium-ion battery parameters.

Parameters	Numerical value
Nominal capacity (Ah)	15
Nominal voltage (V)	3.2
Cell mass (kg)	0.35
Cell dimensions (mm)	140 × 65 × 18
Resistance (mΩ)	4
Charge upper limit voltage (V)	3.65
Charging current (C)	0.5
Discharging cut-off voltage (V)	2.25

Table 2
Heat production at different discharge rates.

Discharge rate (C)	Heat generated of battery cell (W)
0.5	1.08
1	2.61
1.5	4.59
2	7.02
2.5	9.90

respectively, compared with the unidirectional air cooling at 3 C discharge rate. Zhuang et al. [22] proposed a reciprocating flow BTMS to homogenize the cell temperature distribution. The results revealed that the shorter the reciprocating cycle time was, the better the temperature uniformity of battery pack was. Considering the power consumption, the optimal time was at a reciprocating cycle of 400 s.

The battery cell spacing is the critical parameter of the air cooling

technologies and has attracted more attention of scholars. Chen et al. [23] optimized the battery spacing through the flow resistance network model and improved the cooling efficiency of parallel air-cooled BTM. Kumar et al. [24] studied the influences of horizontal and longitudinal battery spacing, and found that the horizontal battery spacing had a great influence on the cooling efficiency of the battery package, and a reasonable longitudinal battery spacing could improve the temperature uniformity. Using surrogate-based optimization, Liu et al. [25] divided 11 channel spaces into 4 groups to optimize the battery spacing for better cooling performance. Li et al. [26] introduced a composite BTMS that used a combination of silica cooling plates and a copper mesh attached to both sides of the battery for air cooling to improve the thermal performance of the BTMS.

A variety of work has been done by scholars to optimize the architecture of air-cooled battery thermal management systems. Liu et al. [27] proposed a novel J-type air cooling BTMS by integrated the U- and Z-type configurations and the cooling performance was compared. Meanwhile, some scholars had added spoiler in BTMS to change the air flow direction in the system, so as to improve the temperature distribution of the battery. Zhang et al. [28] proposed a novel optimization method of adding spoilers in the distribution manifold and entrance of some channels. It was found that the air flow in the cooling channel could be more uniform by this method, so as to the temperature difference between the battery pack was reduced. Based on Ref [28], Wang et al. [29] discussed the number of spoilers on the heat dissipation performance of the BTMS.

Meanwhile, it is vital to choose the appropriate and correct structural parameters, which have a great impact on the heat dissipation of BTMS. Thus, scholars have made a lot of attempts and researches in this area to improve the cooling performance. Hou et al. [30] analyzed the structural parameters of BTMS by introducing the field synergy equation and combining the flow resistance network model, and optimized the channel spacing and the structural parameters of the outlet plenum of BTMS. The simulation results indicated that the optimized ΔT_{max} decreased by more than 56%. Chen et al. [31] adopted the flow resistance model and multi-objective genetic algorithm to optimize the battery spacing, angle and width of inlet and outlet manifold, inlet flow rate. The results depicted that the BTMS after optimizing could reduce the power consumption, maximum temperature difference and maximum temperature by 16.7%, 60.7% and 3.4 K, respectively. E et al. [32] explored different air cooling strategies through setting air flow inlet and outlet on the top, bottom and side of the battery box.

Scholars have found through their research that the method of adding secondary outlet has a great influence on the cooling performance of BTMS, and the heat dissipation effect can be greatly improved. Park [33] analyzed the influences of the layout form of inlet and outlet,

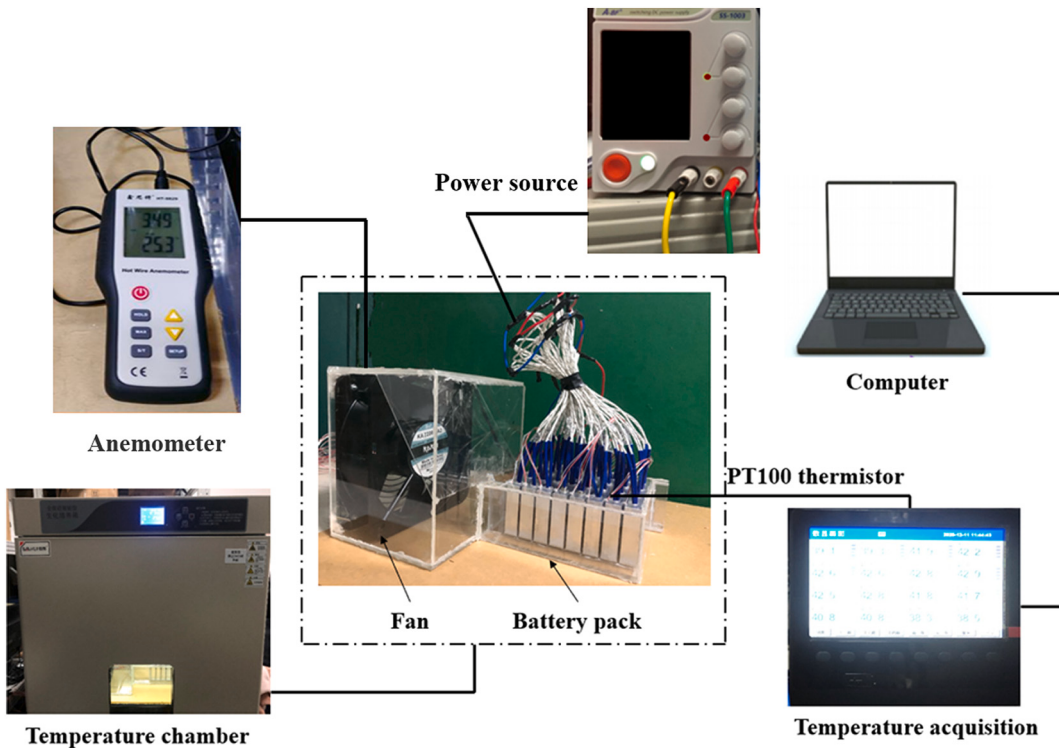


Fig. 3. Schematic of battery pack testing system.

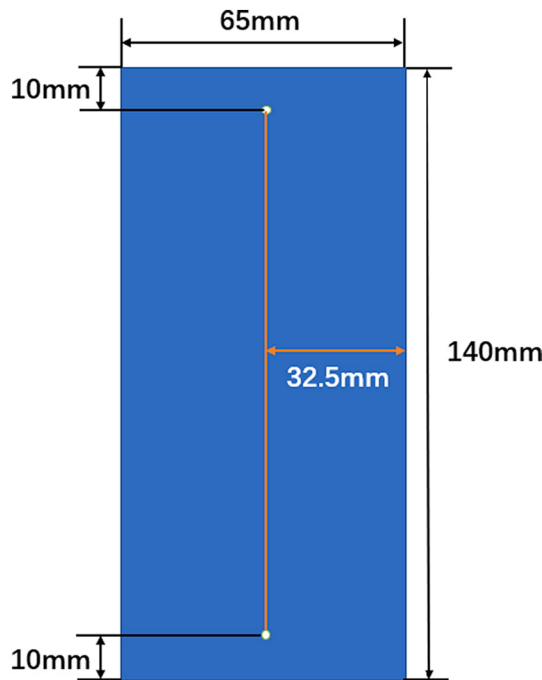


Fig. 4. Position of measuring points.

the height of manifold and the setting of secondary air outlet on the cooling performance of BTMS. Hong et al. [34] improved the cooling performance by adding the secondary vent, and further discussed the effects of the position and size of the secondary vent on the heat dissipation performance of the BTMS. Shahid et al. [35] added a transverse

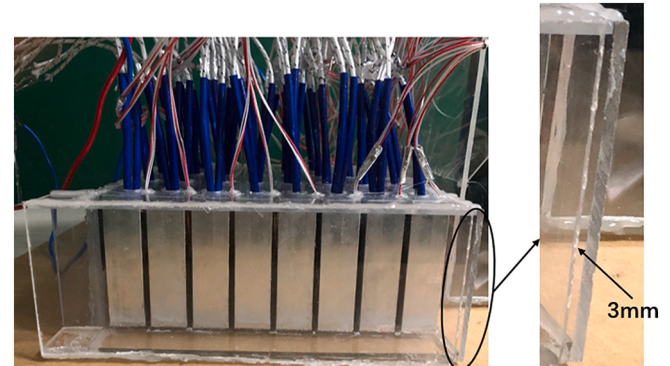


Fig. 5. Schematic of secondary outlet.

secondary inlet to change the flow direction and to remove the dead flow area behind the cells, so as to provide a uniform flow distribution in the system. However, the existing literatures mainly focuses on analyzing the effectiveness of the secondary vent and optimizing the parameters of a single secondary vent. So, it is necessary to further analyze the influences of relevant parameters of secondary outlet on cooling performance, such as quantity, position and width. Therefore, in this study, a Z-type parallel air-cooled model with indefinite quantity secondary outlets were developed. Combined with CFD method, the influences of the position, number and width of the secondary outlets on the cooling performance of BTMS are investigated. Then, according to the temperature distribution of battery cells, the optimum BTMS based on the above will be further optimized by adding the baffles in some cooling channels to better the uniformity of temperature distribution of battery pack.

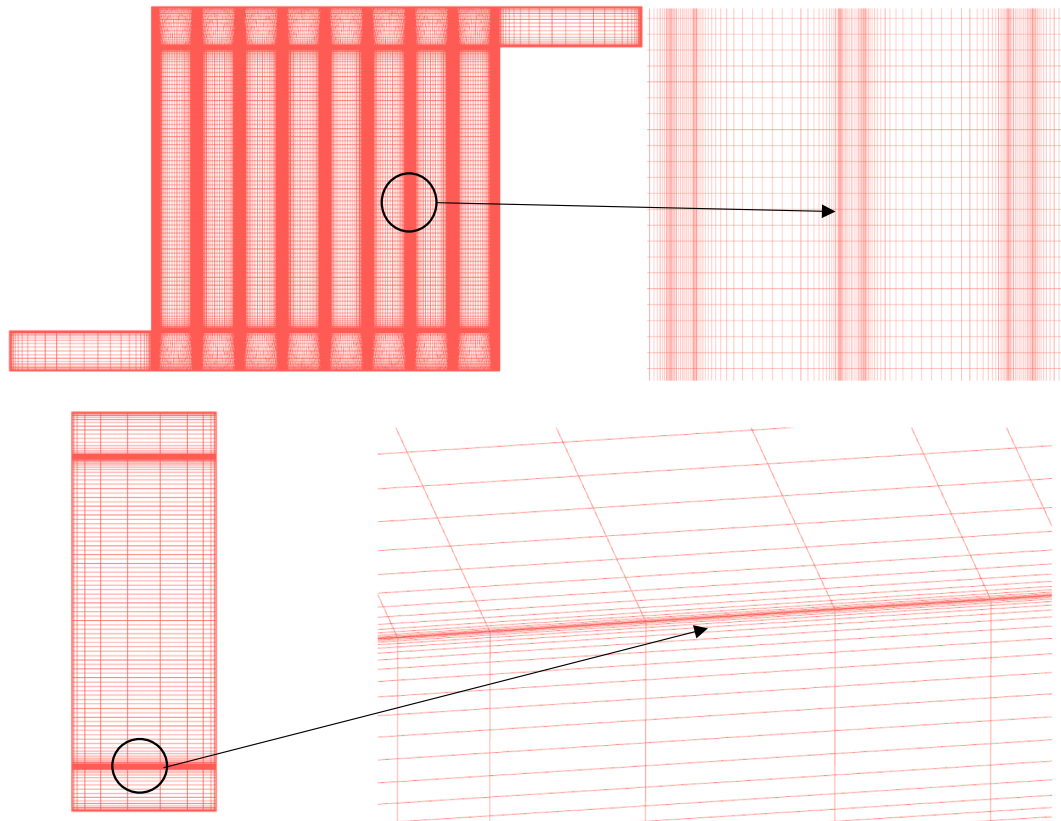


Fig. 6. Structured grid and boundary layer.

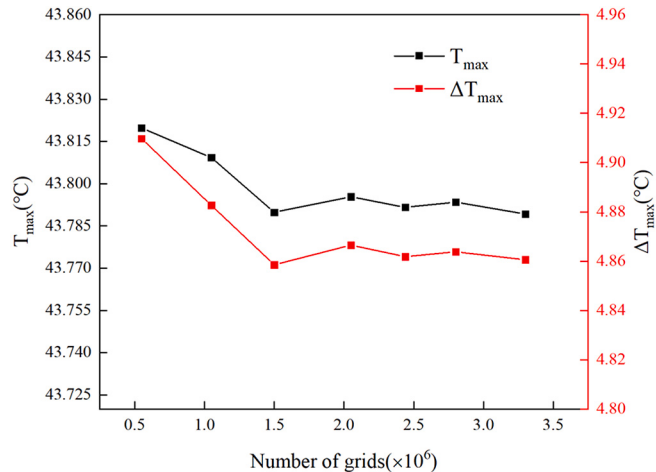


Fig. 7. Simulation results under different grid numbers.

2. Model

2.1. Illustration of the parallel air-cooled BTMS

Air cooling BTMS of the Z-type parallel represented in Fig. 1 was adopted in this work. The parameters of the battery pack model were shown in Fig. 2, included 8 cells and 9 cooling channels, and the batteries were attached to both sides of the battery box. The length of the battery L₁ was 65 mm, the width W₁ was 18 mm and the height H₁ was 140 mm. The inlet width (W_{in}) and outlet width (W_{out}) were 20 mm, the

Table 3
Properties of air, battery [38], and acrylic wall.

Property	Air	Battery (lithium)	Battery (aluminum)	Acrylic wall
Density ($\text{kg}\cdot\text{m}^{-3}$)	1.165	2136.8	2700	1.2×10^3
Specific heat ($\text{J}\cdot\text{kg}^{-1}\cdot\text{K}^{-1}$)	1005	1633	900	0.35
Dynamic viscosity ($\text{kg}\cdot\text{m}^{-1}\cdot\text{s}^{-1}$)	1.86×10^{-5}	—	—	—
Thermal conductivity ($\text{W}\cdot\text{m}^{-1}\cdot\text{K}^{-1}$)	0.0267	$1(\lambda_{b,z}), 29(\lambda_{b,x}), 29(\lambda_{b,y})$	240	1.4
Volume heat source ($\text{W}\cdot\text{m}^{-3}$)	—	60,439.56	60,439.56	—
Size ((H_1) mm \times ($W_1)$ mm \times ($L_1)$ mm)	—	18 \times 65 \times 140	18 \times 65 \times 140	—

inlet length (L_{in}) and outlet length (L_{out}) were 70 mm, and the width (d) of each cooling channel was 3 mm.

2.2. Experiment

2.2.1. Charge and discharge experiment of lithium-ion battery cell

For the square lithium iron phosphate battery studied in this paper, detailed battery parameters were shown in Table 1. Our team conducted constant-current and constant-voltage charging and discharging experiments on square lithium iron phosphate batteries to obtain the average temperature rise curves at each discharge rates, and the specific experimental platform and experimental process were referred to Ref [36]. and according to the formula,

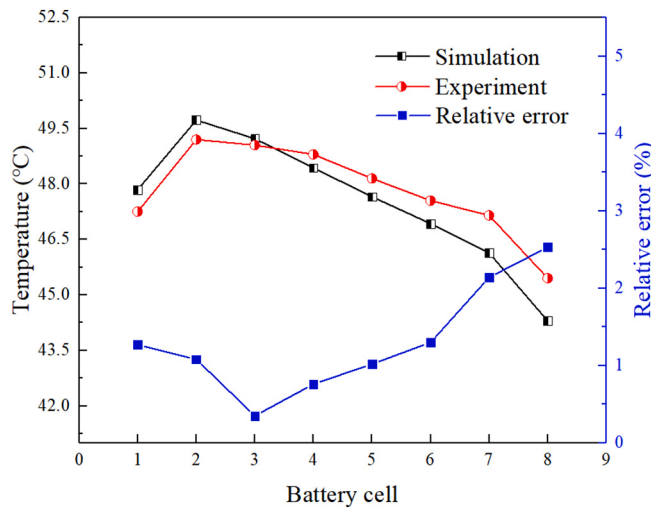


Fig. 8. Comparison of experimental and simulated battery temperatures (3 m/s).

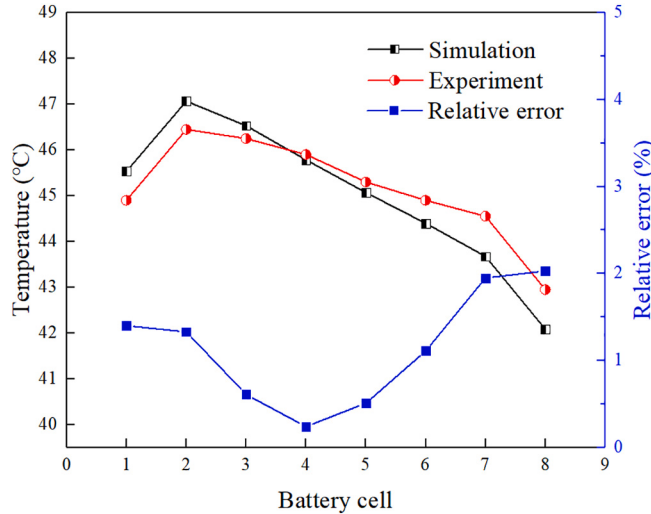


Fig. 9. Comparison of experimental and simulated battery temperatures (3.5 m/s).

$$Q_1 = I^2 R + IT \frac{\partial U_{ocv}}{\partial T} \quad (1)$$

$$Q_2 = mC_p \frac{dT}{dt} \quad (2)$$

$$\frac{1}{I} \frac{dT}{dt} = \frac{R}{mC_p} \cdot I + \frac{1}{mC_p} \cdot T \cdot \frac{\partial U_{ocv}}{\partial T} \quad (3)$$

$$\frac{dT}{dt} = 7 \times 10^{-6} I + 2 \times 10^{-4} \quad (4)$$

$$Q = mC_p \frac{dT}{dt} = 4 \times 10^{-3} I^2 + 0.114I \quad (5)$$

where Q_1 is the heat generated by the battery, Q_2 is the heat absorbed by the battery. Discharge the battery at each discharge rate for 15 min to obtain $\frac{dT}{dt}$, thus, the relationship between $\frac{1}{I} \frac{dT}{dt}$ and I can be fit as Eq. (4).

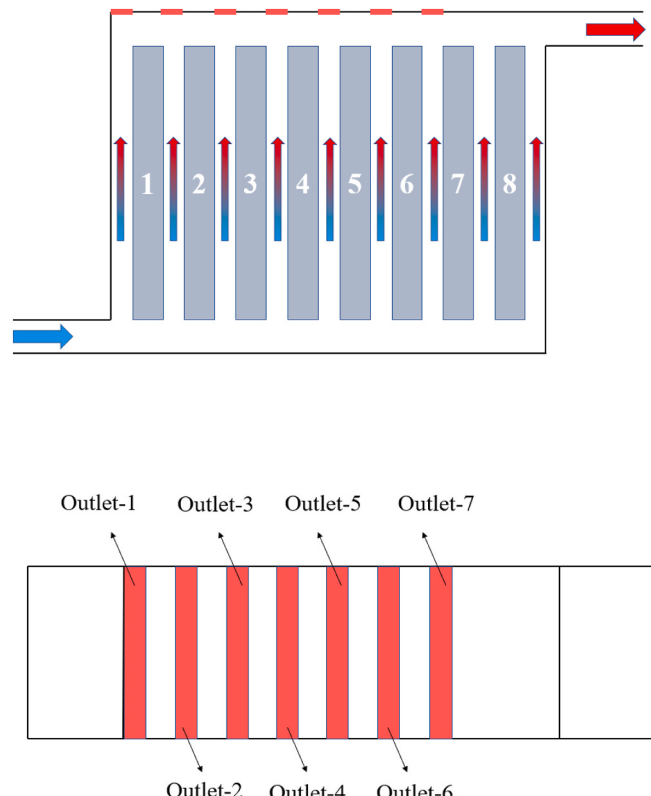
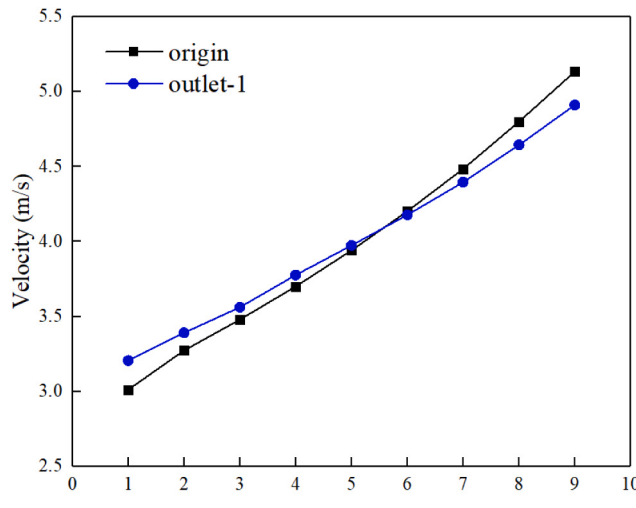


Fig. 10. Positions of the secondary outlet.

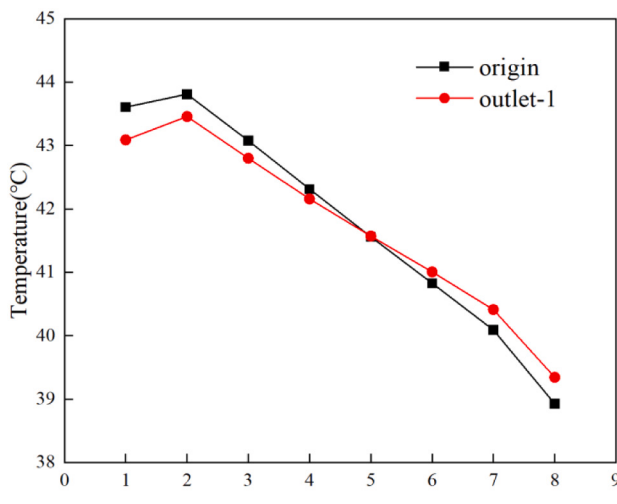
and further obtain the specific heat capacity of the battery is 1633 J/(kg·K). Combined with Eqs. (2) and (4), obtain heat production Eq. (5). According to the heat generation formula, the heat generation of the battery under different discharge rates is obtained, so the volumetric heat source of the battery is obtained. The heat generation at the discharge rate of 0.5 C to 2.5 C was shown in Table 2.

2.2.2. Experiment on air cooling heat dissipation of lithium-ion battery pack

The experimental platform in Fig. 3 was built to test the heat dissipation of Z-type battery pack. The battery box was made of acrylic plates. The battery was replaced by aluminum block and heating rod, and each aluminum block was inserted with 4 heating rods. The heating rods were connected with the DC power supply (SS-1003, 3A/100 V, Dongguan Bufan Electronics Co. Ltd., China) after parallel connection. The operation of the fan was directly determined by the DC power supply, and the air flow at the inlet was measured by a specific anemometer (HT-9829, Shenzhen Lai Xun Technology Co., Ltd., China). Two PT100 thermal resistance were pasted on the surface of each battery, and the pasting positions of PT100 thermal resistance were shown in Fig. 4. Each PT100 thermal resistance was connected with the temperature acquisition instrument (MIK-R6000C, Hangzhou Mike Sensing Technology Co. Ltd., China), and the battery temperature was collected at any time by the temperature acquisition instrument. Here, the temperature of the battery was represented by the average of two measuring points. During the air cooling experiment of battery pack, the ambient temperature remained constant. In order to meet the requirements of the experiment, the battery package was placed in a temperature chamber (SPX-350, Guangzhou Baihui Technology Co. Ltd., China), and the temperature could be adjusted from 0 °C to 60 °C, with an accuracy of ±0.5 °C.



(a) Velocity



(b) Temperature

Fig. 11. Simulation results of the original model and outlet-1 model.

Compared with the model described in Section 2.1, a secondary outlet with a width of 3 mm and a length of 65 mm was added in the cooling channel 1 of the battery package model. As shown in Fig. 5, due to the size limitation of the incubator, the length of the inlet and outlet was shorten to 20 mm, and other parameters were completely consistent. Moreover, according to Ref [20], the change of inlet and outlet length had little effect on the cooling performance of BTMS. The initial conditions of the experiment were that the experimental ambient temperature was set to 25 °C, the discharge rate was set to 2.5 C and the inlet air flow rate were set to 3 m/s and 3.5 m/s. Due to the limited power of the small fan used in the experiment, the air inlet of the air-cooled model of the battery pack was too small, and the maximum air inlet speed in the experiment could only reach 3.5 m/s. Therefore, the wind speeds of 3 m/s and 3.5 m/s were used for comparative verification in experiments and numerical simulation.

2.3. Computational model

2.3.1. Grid generation and grid dependence analysis

It was an effective way of the CFD software ANSYS ICEM to be used to mesh the model in this work. The structured grid and boundary layer grid were shown in Fig. 6. In this model, the Reynolds number calculated by the inlet velocity was greater than 2300, so the airflow state in BTMS was turbulent flow, and the value of Y^+ needs to be close to 1. Moreover, the purpose of setting the height of the first layer grid to 0.1 mm was to ensure the simulation accuracy and facilitate the subsequent simulation calculation. Because the number of grids has a certain effect on the simulation results, so the grid size of battery package model needs to be determined by grid independence analysis in CFD simulation. The T_{\max} and ΔT_{\max} of the BTMS under different number grids were illustrated in Fig. 7. Obviously, with the increase of the number of grids, T_{\max} and ΔT_{\max} changes little, once the number of grids was greater than 1.05×10^6 , the T_{\max} and ΔT_{\max} is almost constant, and its value changed less than 0.05 °C. Therefore, the grid number of 1.05×10^6 was chosen for the mesh generation for all the models involved in this work, which could not only meet the accuracy requirements, but also reduced the time cost.

2.3.2. Computational fluid dynamics

This paper used CFD method to calculate the velocity field and temperature field of BTMS. The flow in this paper was turbulent, and the N-S equation of k-ε turbulence model was selected to simulate the flow circulation in the system. Here is the governing equation [37]:

For the area of airflow,

$$\frac{\partial u_i}{\partial x_i} = 0 \quad (6)$$

$$\rho_a u_j \frac{\partial u_i}{\partial x_j} = - \frac{\partial p}{\partial x_i} + \frac{\partial}{\partial x_j} \left[(\mu + \mu_t) \frac{\partial u_i}{\partial x_j} \right] \quad (7)$$

$$\rho_a C_{p,a} \frac{\partial T_a}{\partial t} + \rho_a C_{p,a} u_j \frac{\partial T_a}{\partial x_j} = \frac{\partial}{\partial x_j} \left[\left(\lambda_a + \frac{\mu_t}{\sigma_T} \right) \frac{\partial T_a}{\partial x_j} \right] \quad (8)$$

where u_i, u_j are air velocity components, p is Reynolds average pressure, μ_t is turbulent viscosity coefficient, $C_{p,a}$ is air specific heat capacity, T_a is air temperature, λ_a is air thermal conductivity, σ_T is turbulence model parameter. In addition, the energy conservation equation of the battery can be expressed as follows:

$$\rho_b C_{p,b} \frac{\partial T_b}{\partial t} = \nabla \cdot (\lambda_b \nabla T_b) + q \quad (9)$$

where ρ_b , $C_{p,b}$, T_b , λ_b , and q are the density, specific heat capacity, temperature, thermal conductivity and the heat generation of lithium battery, respectively.

The air was set as the fluid domain, the battery was set as the solid domain, and the material was set as lithium (in the experiment of cooling battery pack by means of air, the aluminum block and heating rod were used to replace the battery, so the material of the battery was set as aluminum in the simulation verification, but the material of the battery was set as lithium in the subsequent optimization simulation calculation), the corresponding body heat source was loaded, and Table 3 showed the properties of the air, battery and acrylic wall. For finding the solution of governing equation, appropriate boundary conditions and initial conditions must be set. Here, the inlet velocity was set as the inlet condition, and the standard atmospheric outlet was set as the outlet condition. The ambient temperature was 25 °C, the air inlet velocity in subsequent optimization was 4 m/s, and the ambient temperature was the same as the inlet air temperature. The wall was chosen as adiabatic non slip wall since the Y^+ value was small [38], it is suitable to choose the wall function as the reinforcement wall and select the SIMPLE algorithm to find the solution of equation. The discretization of

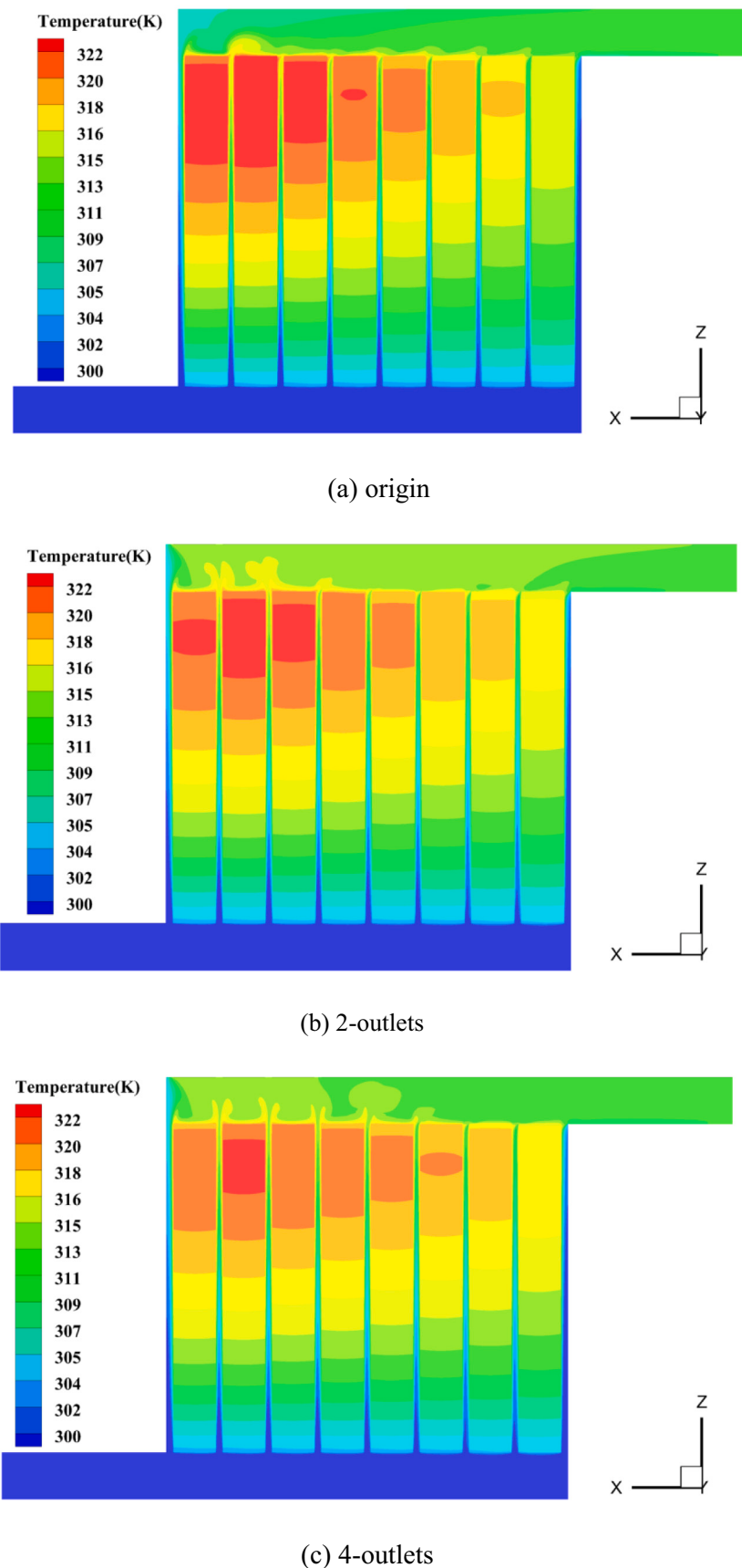
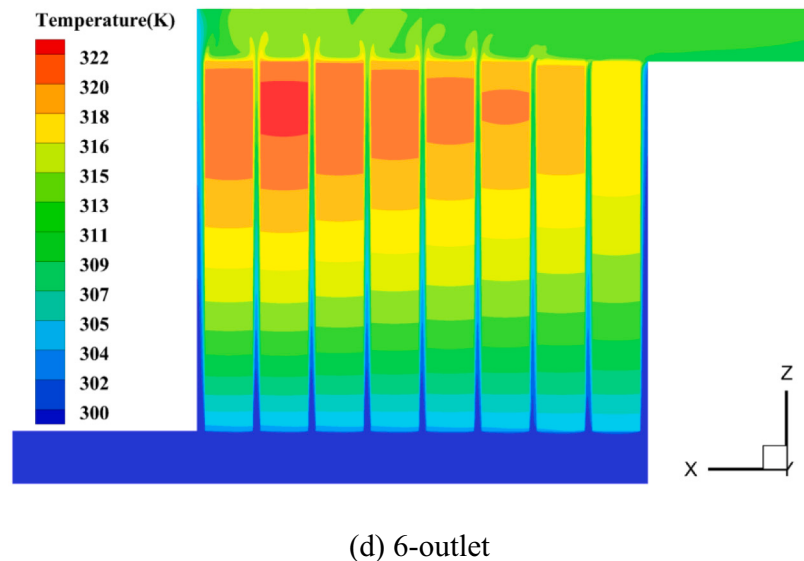
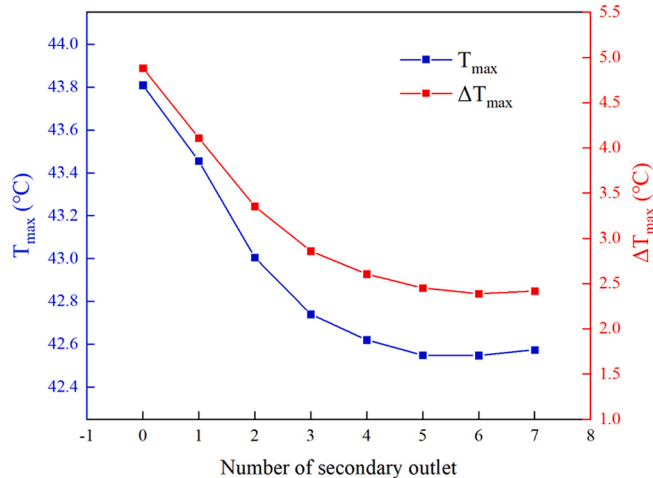


Fig. 12. Temperature contour of the model with different number secondary outlets.



(d) 6-outlet

Fig. 12. (continued).

Fig. 13. T_{\max} and ΔT_{\max} of the model with different number of secondary outlets.

momentum, energy and pressure were chosen as the second-order upwind, and convergence residuals of the governing equations were set to 10^{-6} . The commercial software FLUENT was used to solve the governing equations and simulate the air-cooled system.

2.3.3. Comparison of experimental results and simulated results

Fig. 8 and Fig. 9 show the comparison of the experimental and simulated battery temperatures when the ambient temperature was 25 °C, the discharge rate was 2.5 C and the inlet air velocity was 3 m/s and 3.5 m/s, respectively. It can be found that the battery temperature obtained by experiment and simulation showed the same trend, and the errors of each battery temperature were within 2.6%. It is indicated that the CFD method and model in this paper was accurate and effective.

3. Results and discussion

3.1. Effect of secondary outlet number

The position of the secondary outlet was shown in Fig. 10. In this section, the width of the secondary outlet was 3 mm (which was equaled

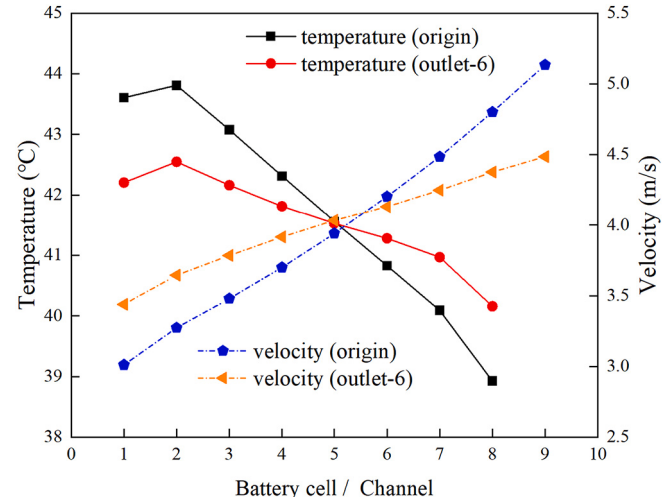


Fig. 14. Battery temperature and airflow velocity in cooling channel of origin and 6-outlet model.

to the spacing between the batteries of the model) and the length was 65 mm (which was equaled to the length of the battery box). As shown in Fig. 10, the secondary outlets were set at the top of the collecting manifold against the cooling channel by symmetrical arrangement. The secondary outlet for No i cooling channel was denoted as “Outlet-i” ($i = 1, 2, \dots, 7$).

3.1.1. Comparative analysis with original model

Fig. 11 shows the comparison between the simulation results of the original model and the model with outlet-1 added. It can be seen from Fig. 11 (a) that the air velocity at the outlet of the original model was much higher than that at the inlet, and the air velocity difference between channel 9 and channel 1 was as high as 2.12 m/s. As a result, the battery temperature near the inlet is higher than that near the outlet in the original model. After adding outlet-1, the airflow velocities for channel 1 to channel 5 were increased, conversely, the airflow velocities for channel 6 to channel 9 were decreased. Meanwhile, the maximum velocity difference between each channel was reduced to 1.71 m/s, which showed the airflow velocity distribution in the cooling channels

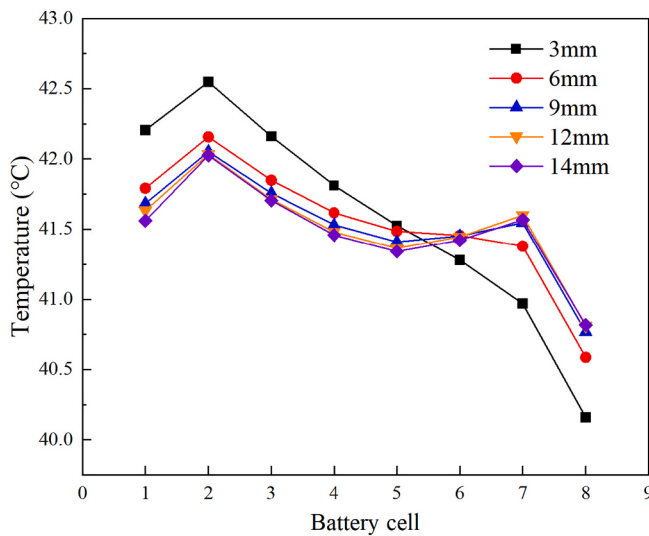


Fig. 15. Battery cell temperature of different width of secondary outlet.

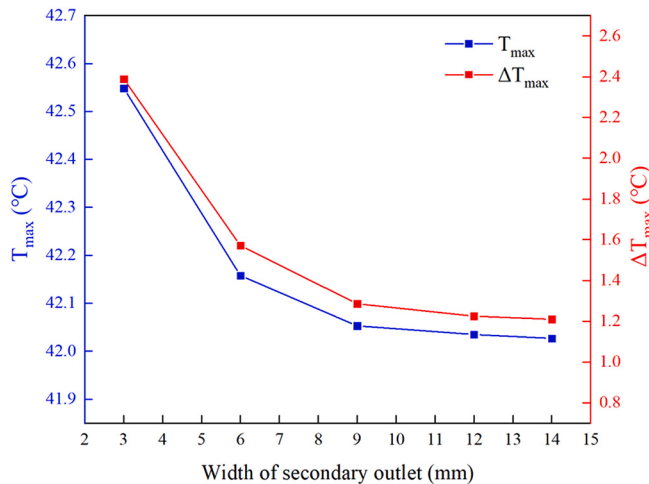


Fig. 16. T_{max} and ΔT_{max} of different width of secondary outlet.

became more even. Fig. 11 (b) shown the temperature values of each cell in the original model and when the outlet1 was added. Compared with the original model, T_{max} and ΔT_{max} of the model with one secondary outlet model were significantly reduced. It is clearly demonstrated that the heat dissipation performance and the uniform of temperature distribution of the BTMS were significantly improved by adding secondary outlet in the model.

3.1.2. Comparative analysis of secondary outlets number

The influence of different number of secondary outlets on the cooling performance of BTMS was studied in this section. When the secondary outlet number was N ($N = 1, 2, \dots, 7$), which was denoted as “N-Outlets” ($N = 1, 2, \dots, 7$). Moreover, it depicted that the N secondary outlets consisted of outlet-1 to outlet-N. Battery temperature, T_{max} and ΔT_{max} under different number of secondary outlets are shown in Fig. 12 and Fig. 13. It shows that with the increase of the number of secondary outlets, the battery temperature, T_{max} and ΔT_{max} of the battery pack generally showed a downward trend. At the same time, when the number of secondary outlets was 6, namely 6-outlet model, the best cooling performance of the BTMS was achieved. Compared with the

initial model, T_{max} and ΔT_{max} were reduced by 1.26 °C (2.81%) and 2.49 °C (51.07%), respectively. Besides, when the number of the secondary outlets was no more than 6, T_{max} and ΔT_{max} were decreased gradually with the increase of secondary outlets. Fig. 14 depicts the airflow velocities in the cooling channels and temperatures of battery cells for the original model and 6-outlet model, respectively. The comparison curves of airflow velocity showed that the velocities of channel 1 to 5 increased obviously, conversely, those of channel 6 to 8 decreased obviously. Similarly, the comparison curves of battery temperature depicted that the temperatures of battery 1 to 4 decreased, while the temperature of battery 6 to 8 increased. The primary reason for the above phenomenon was that the secondary outlets reduced the pressure of the convergence plenum around them, thereby making the velocity distribution of the BTMS more uniform. Therefore, the 6-outlet model would be set as base-model to further investigate in the follow sections.

3.2. Effect of secondary outlet width

From the knowledge of fluid dynamics, the width of secondary outlet will affect the distribution of the velocity and pressure of airflow. Hence the effect of the width of the secondary outlets would be discussed in this section for the 6-outlet model. Since there was no extra space on the left side of outlet-1 for symmetrical arrangement, outlet-1 expanded the increased width to the right side to meet the width requirements when the width of outlet-1 was greater than 3 mm.

3.2.1. Comparative analysis of different secondary outlets width

In this section, the effect of the width of the secondary outlets was discussed. The width was 3 mm, 6 mm, 9 mm, 12 mm and 14 mm respectively. Fig. 15 demonstrates the temperature curves of battery temperature of the above five models. It can be observed that the temperatures of battery 1 to 5 were decreased with the increase of the width for secondary outlet. While, the temperatures of battery 6 to 8 were increased when the widths exceeded 3 mm. Fig. 16 displays T_{max} and ΔT_{max} of the model with different width of secondary outlet. It could be found that with the increase of the width of secondary outlet, T_{max} and ΔT_{max} of the battery pack were decreased, but the temperature drop was greatly reduced when the width was greater than 9 mm. The results showed that the effect of the variation of the secondary outlet width on the thermal performance of the battery pack was relatively more complex. Therefore, the width combination of the secondary outlets would be further discussed to obtain the best cooling performance for the BTMS.

3.2.2. Comparative analysis of different secondary outlets width combination

In the previous section, the influences of the secondary outlets with equal width on the cooling performance of BTMS were analyzed, and the influences of the six secondary outlets with different width on the cooling performance of the BTMS would be investigated in this section. Based on the results obtained in the above sections, the widths of the six secondary outlets were considered as the optimization variables and divided into three groups: Group A contained outlet-1, outlet-2 and outlet-3; Group B contained outlet-4 and outlet-5; and Group C contained only outlet-6. According to the rules of fluid dynamics and the distribution characteristics of battery temperature, the width of the secondary outlet neared the inlet should be set to the maximum and then decreased in turn. Thus, the width of Group A (W_A) was set to 9 mm, 12 mm and 14 mm, the width of Group B (W_B) was set as 6 mm and 9 mm, the width of Group C (W_C) was 3 mm. All cases were denoted as “ $W_A-W_B-W_C$ ”. The temperature distribution of the model with different width combinations and the curves of T_{max} and ΔT_{max} of the BTMS are illustrated in Fig. 17 and Fig. 18. Finding that the differences of T_{max} and

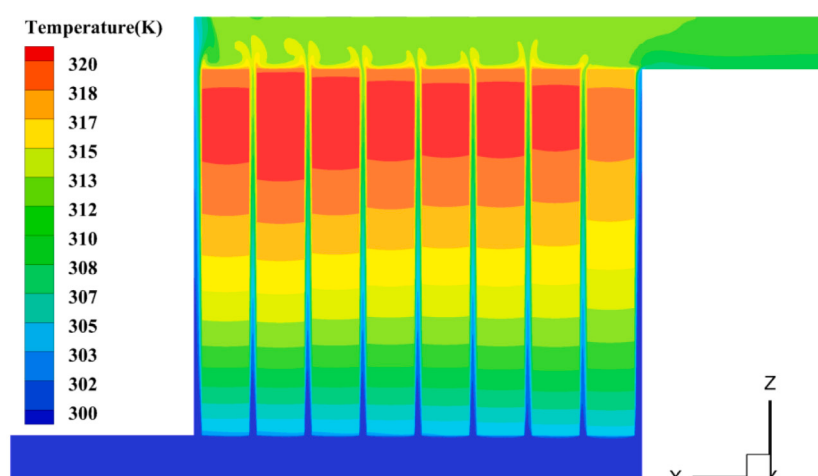
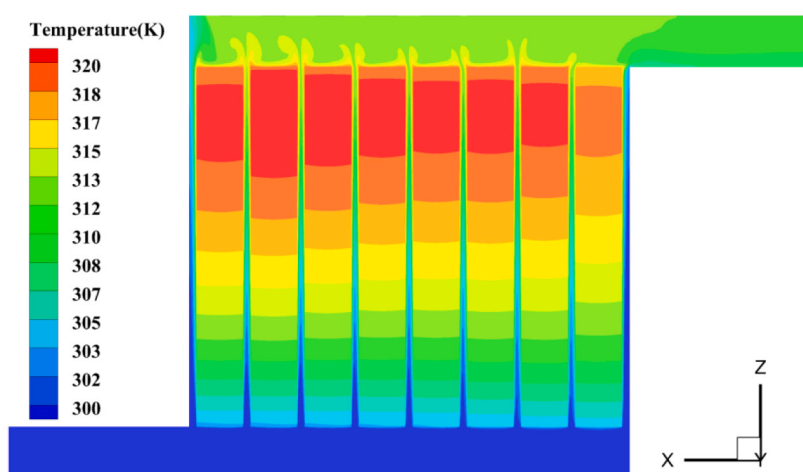
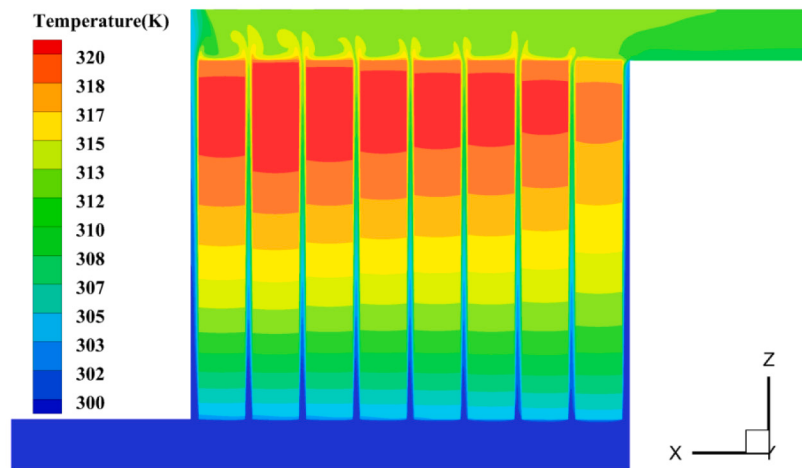


Fig. 17. Temperature contour of the model with different width combination.

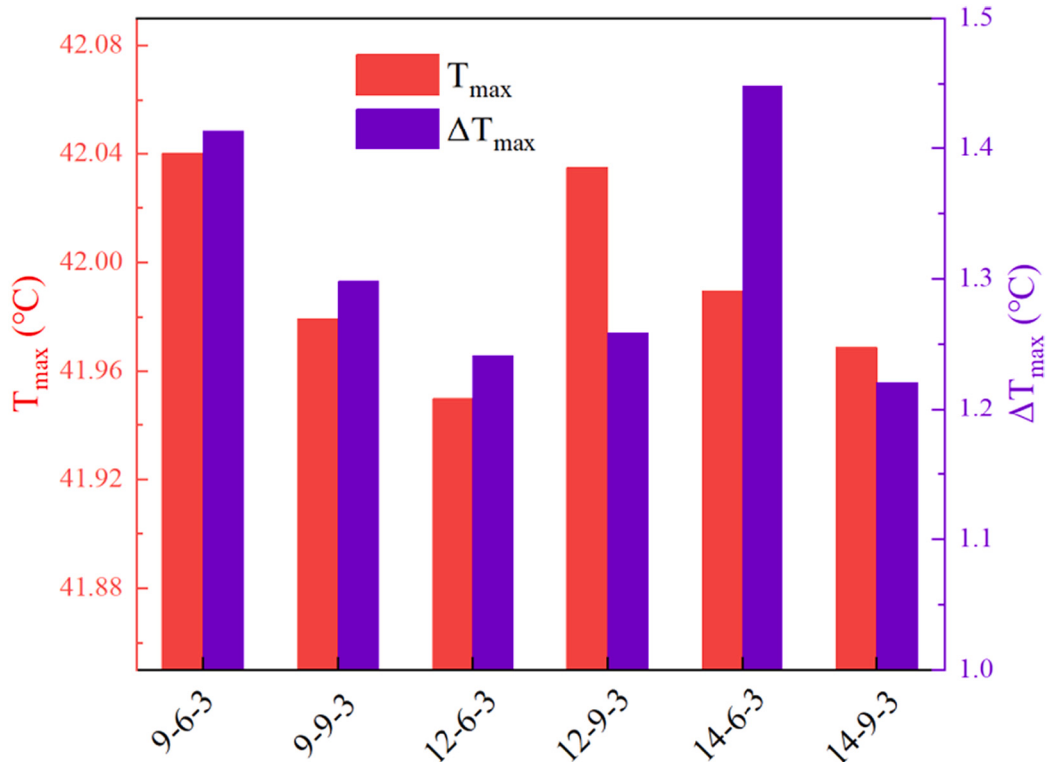


Fig. 18. T_{\max} and ΔT_{\max} of the model with different width combination.

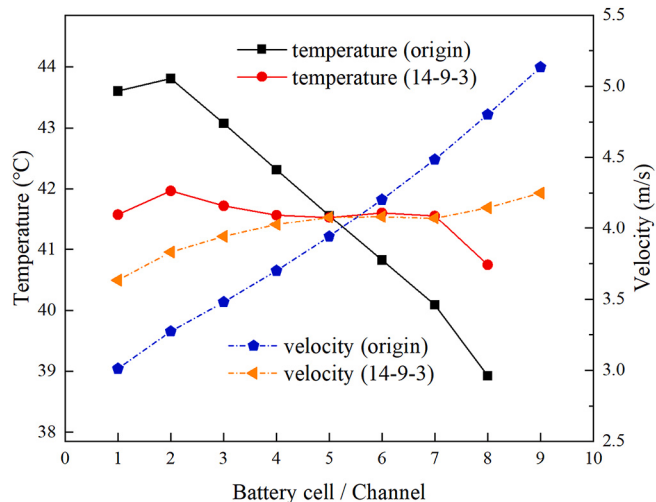


Fig. 19. Battery temperature and airflow velocity in cooling channel of origin and 14-9-3.

ΔT_{\max} in the 6 cases were relatively small. Among them, the composite cooling performance of the 14-9-3 model was better. Compared with the original Z-type BTMS, T_{\max} was reduced by 1.84 °C (4.20%) and ΔT_{\max} was reduced by 3.66 °C (75%). Fig. 19 is a diagrammatic representation of the temperature value for each battery and the airflow velocity for each channel under the original model and the 14-9-3 model. It is obvious that the temperature and velocity distribution of the battery pack tended to be uniform under 14-9-3 conditions. In addition, it is known from the findings of Hong et al. [34] that the location set on the

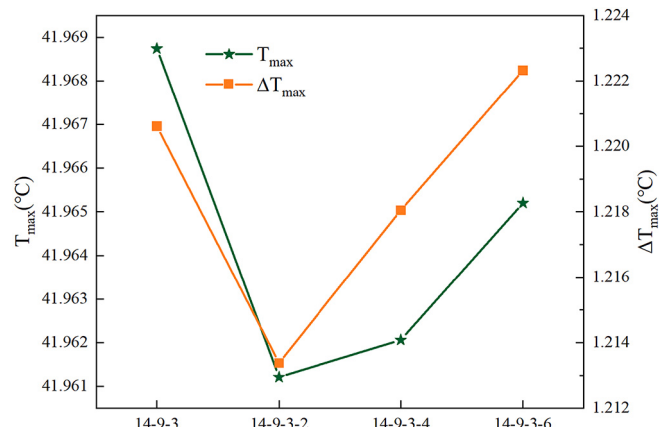


Fig. 20. T_{\max} and ΔT_{\max} of added a different widths secondary outlet on the side based on the 14-9-3.

side had better cooling performance when there was only one secondary vent.

Based on this, after discussing the setting of the top secondary outlet, based on the 14-9-3 model, we attempted to add a secondary outlet with dimensions of 2 mm, 4 mm and 6 mm on the side, expressed as 14-9-3-2, 14-9-3-4 and 14-9-3-6, respectively. The simulation results are shown in Fig. 20. It can be seen from the figure that adding a secondary vent on the side had little effect, and the maximum temperature difference was only 0.04 °C. To sum up, since the 14-9-3 condition had the best performance, this condition would be taken as the base-model to further investigate. For simplifying in next section, the base-model 14-9-3 was denoted as BM-1493.

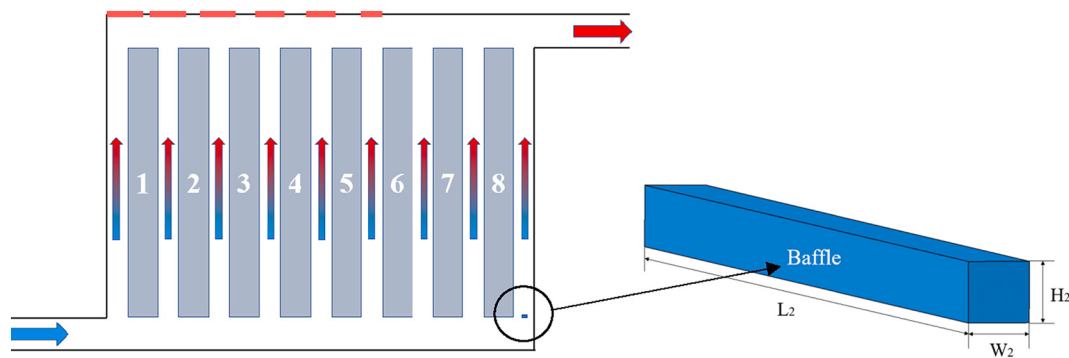


Fig. 21. Positions and shape of the baffle.

3.3. Optimization of the baffle in cooling channel

It is obvious that the temperature of battery 8 was lower than those of other batteries in Fig. 17(c) and Fig. 19. In order to improve the airflow distribution of BM-1493, a baffle was set in cooling channel 9, as shown in Fig. 21. The baffle width (W_2) was set to 0.5 mm, 0.7 mm, 0.9 mm, 1 mm, 1.1 mm, 1.2 mm and 1.3 mm, and the height (H_2) was 0.5 mm, and the length (L_2) was 65 mm. After adding the baffle, only the baffle area was set as an adiabatic solid domain wall without slip, and the other CFD boundary conditions were set in the same way as before. Adding the baffle could reduce the air spread in the cooling channel near battery 8, so as to increase the air distribution to other nearby batteries. After that, properly increase the temperature of battery 8 and properly reduce the temperature of other batteries. Therefore, the temperature of the battery 8 could be increased appropriately, and the temperature of other batteries could be reduced to some extent. In this way, the heat dissipation performance of the thermal management system was greatly improved. The setup of the baffle is shown in Fig. 21. The temperature distribution of BM-1493 with different width of the baffle and the variation curves of T_{\max} and ΔT_{\max} were displayed in Fig. 22 and Fig. 23, separately. Finding that when the width of the baffle did not exceed 1.1 mm, T_{\max} and ΔT_{\max} of the battery decreased as the width increased. While, when the width of the baffle was larger than 1.1 mm, T_{\max} and ΔT_{\max} had an upward trend with the increasing of the width of the baffle. In conclusion, when the width of the baffle was 1.1 mm, the BTMS exhibited the optimum cooling performance. Fig. 24 illustrates the comparison curves of airflow velocity in the cooling channels of BM-1493 and the optimum model. We can observe that the airflow velocity in channel 9 was decreased obviously when the baffle was set in. While, the airflow velocities in channel 1 to 8 were increased. Fig. 25 shows the temperature and air velocity curves of the original model, BM-1493 and the optimized model. Compared with the original model, the airflow velocity was more uniform. Compared with BM-1493, except that the airflow velocity of channel 9 was lower, the airflow velocity of channels 1–8 was higher than BM-1493, which made the values of T_{\max} and ΔT_{\max} were reduced to some extent. Compared with the original Z-type BTMS, T_{\max} and ΔT_{\max} decreased by 2.17 °C (4.95%) and 4.49 °C (91.89%), respectively.

4. Conclusion

The flow field and temperature distribution of the battery package were investigated by CFD method in this work. On the basis of the original model, the secondary air outlets were added on the top of the collecting manifold. In order to obtain a more uniform temperature and air flow rate in the BTMS, the secondary outlets and baffle were set on

the top of the collecting manifold and inside the cooling channel, respectively. It was greatly improved for the heat dissipating capability of the BTMS and the homogenization of temperature distribution by optimizing and adjusting the size and number of the secondary outlets and the parameter of the baffle. The following conclusions can be drawn:

1. The reliability of CFD method was proved by the air cooling experiment of battery pack.
2. The number of the secondary outlets had a remarkable effect on the cooling property of the BTMS. When the number of secondary air outlets was 6, the BTMS obtained optimum cooling performance. Results depicted that T_{\max} and ΔT_{\max} were 1.26 °C (2.81%) and 2.49 °C (51.07%) lower than the original Z-type BTMS, respectively.
3. The number and width of the secondary outlets had a large effect on the heat dissipation capacity of the BTMS. The six secondary air outlets were divided into three groups and different width combinations of secondary air outlets were studied. The comprehensive cooling performance of BM-1493 was the best. T_{\max} of the optimal model was reduced by 1.84 °C (4.20%) compared with the previous Z-type BTMS, and ΔT_{\max} was reduced by 3.66 °C (75%).
4. The baffle was placed in some cooling channels of the BTMS to further optimize the performance. Based on the model with the optimal combination of the width of the secondary outlets, the baffle was set in channel 9 to further optimize the cooling performance. The results indicated that when the width of the baffle was 1.1 mm, the BTMS exhibited the optimum cooling performance. T_{\max} was reduced by 2.17 °C (4.95%), and ΔT_{\max} was reduced by 4.49 °C (91.89%), compared with the original Z-type BTMS.

CRediT authorship contribution statement

Furen Zhang: Conceptualization, Methodology, Software, Validation, Writing - Review & Editing, Supervision.

Peiwen Liu: Conceptualization, Methodology, Software, Experiment, Data curation, Formal analysis, Investigation, Data Curation, Writing - Original Draft, Writing - Review & Editing.

Yanxiao He: Conceptualization, Methodology, Software, Experiment, Data curation, Formal analysis, Investigation, Data Curation, Writing - Original Draft, Writing - Review & Editing.

Shiyuan Li: Validation, Writing - Review & Editing.

Declaration of competing interest

The authors declare that there is no conflict of interest.

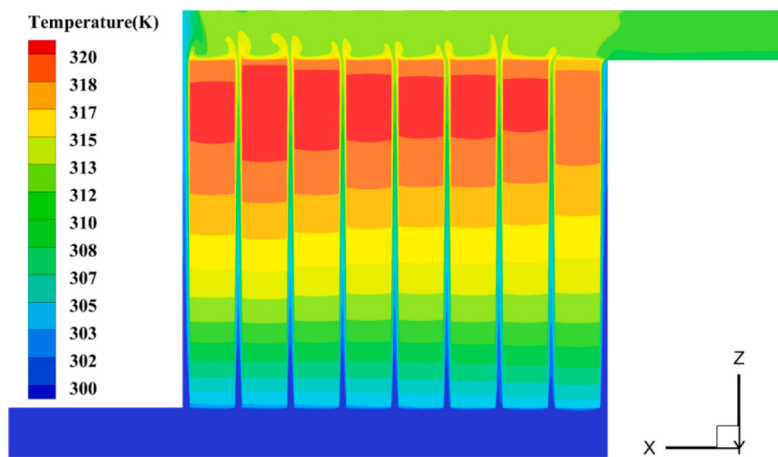
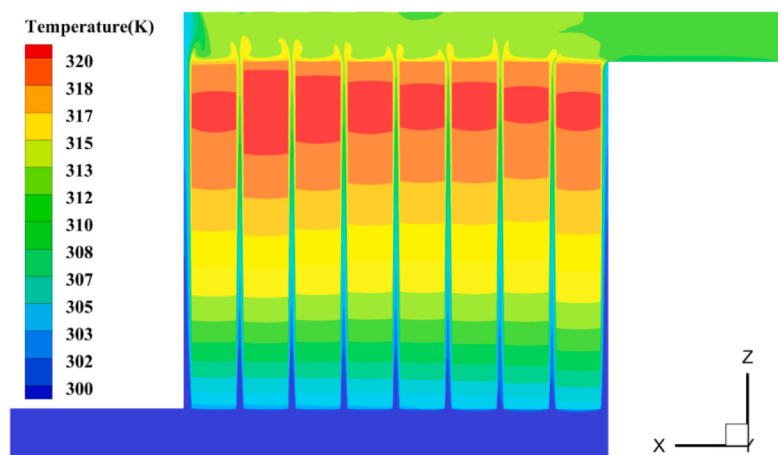
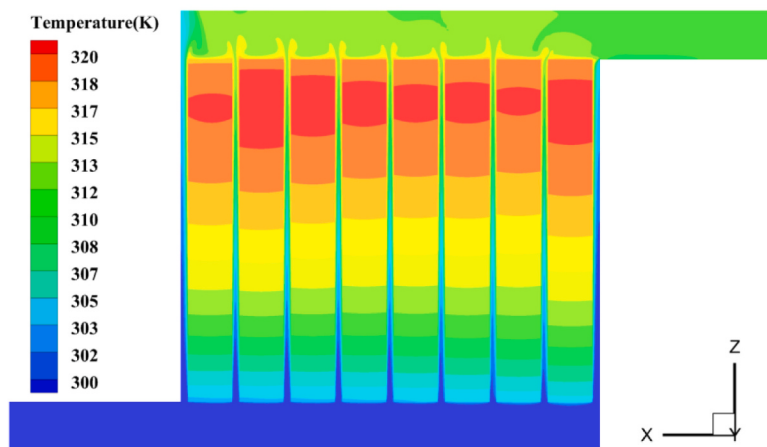
(a) $W_2 = 0.5 \text{ mm}$ (b) $W_2 = 1.1 \text{ mm}$ (c) $W_2 = 1.3 \text{ mm}$

Fig. 22. Temperature contour of BM-1493 with different width of baffle.

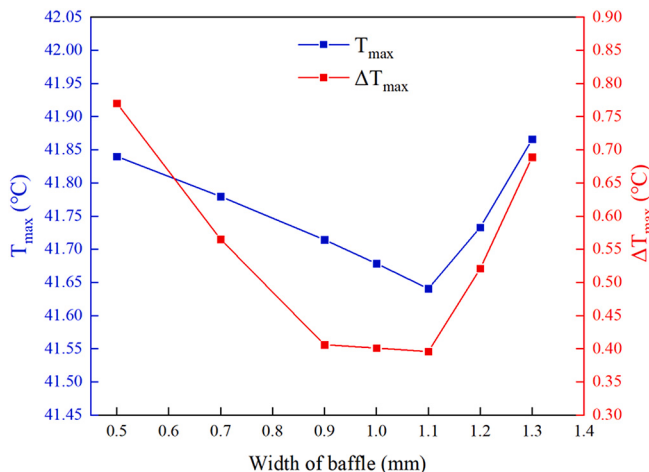


Fig. 23. T_{\max} and ΔT_{\max} of BM-1493 with different width of baffle.

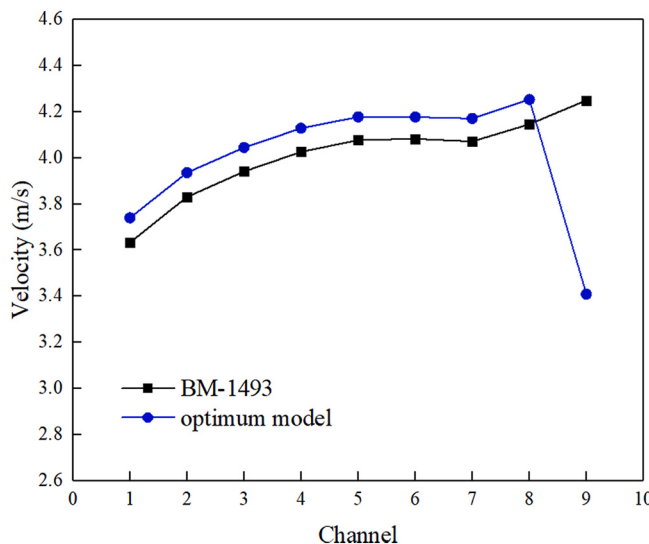


Fig. 24. Airflow velocity in the cooling channel of BM-1493 and optimum model.

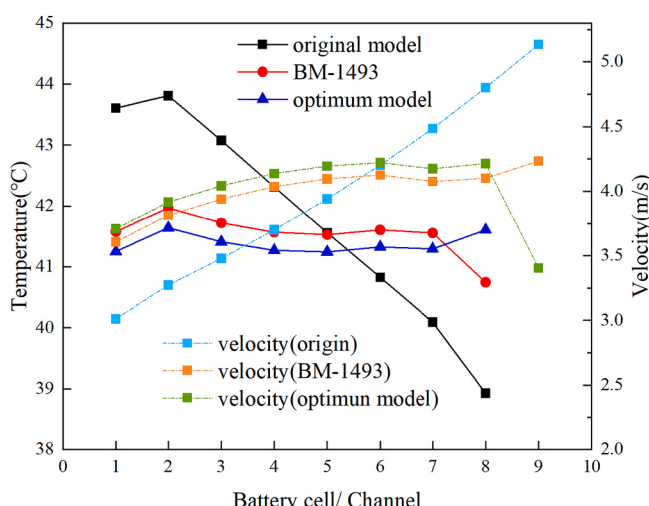


Fig. 25. Battery cell temperature and airflow velocity in cooling channel of original model, BM-1493 and optimal model.

References

- [1] H. Li, Practical evaluation of Li-ion batteries, Joule 3 (2019) 911–914.
- [2] Y. Shi, S. Ahma, H. Liu, K. Lau, J. Zhao, Optimization of air-cooling technology for LiFePO₄ battery pack based on deep learning, J. Power Sour. 497 (2021), 229894.
- [3] Y. Wang, B. Liu, P. Han, C. Hao, S. Li, Z. You, M. Wang, Optimization of an air-based thermal management system for lithium-ion battery packs, J. Energy Storage 44 (2021), 103314.
- [4] F. Zhang, P. Wang, M. Yi, Design optimization of forced air-cooled lithium-ion battery module based on multi-vents, J. Energy Storage 40 (2021), 102781.
- [5] Y. Fan, Y. Bao, C. Ling, X. Tan, S. Yang, Experimental study on the thermal management performance of air cooling for high energy density cylindrical lithium-ion batteries, Appl. Therm. Eng. 155 (2019) 96–109.
- [6] Y. Zhi, J. Zhang, Design a J-type air-based battery thermal management system through surrogate-based optimization, Appl. Energy 252 (2019), 113426.
- [7] H. Zhou, F. Zhou, L. Xu, J. Kong, Q. Yang, Thermal performance of cylindrical Lithium-ion battery thermal management system based on air distribution pipe, Int. J. Heat Mass Transf. 131 (2019) 984–998.
- [8] Y. Fan, Z. Wang, T. Fu, H. Wu, Numerical investigation on lithium-ion battery thermal management utilizing a novel tree-like channel liquid cooling plate exchanger[J], Int. J. Heat Mass Transf. 183 (2022), 122143.
- [9] K. Monika, S. Datta, Comparative assessment among several channel designs with constant volume for cooling of pouch-type battery module, Energy Convers. Manag. 251 (2022), 114936.
- [10] S. Chen, M. Antonio, A. Murat, Constructal design in the cooling and hydraulic performance of tube heat sinks, Int. J. Heat Mass Transf. 129 (2021), 105668.
- [11] W. Jiang, J. Zhao, Z. Rao, Thermal performance enhancement and prediction of narrow liquid cooling channel for battery thermal management, Int. J. Therm. Sci. 171 (2022), 107250.
- [12] X. Luo, J. Gu, H. Ma, Y. Xie, A. Li, J. Wang, R. Ding, Numerical study on enhanced melting heat transfer of PCM by the combined fractal fins, J. Energy Storage 45 (2022), 103780.
- [13] Z. Sun, R. Fan, F. Yan, T. Zhou, A. Zheng, Thermal management of the lithium-ion battery by the composite PCM-fin structures, Int. J. Heat Mass Transf. 145 (2019), 118739.
- [14] J. Ho, Y. See, K. Leong, T. Wong, An experimental investigation of a PCM-based heat sink enhanced with a topology-optimized tree-like structure, Energy Convers. Manag. 245 (2021), 114608.
- [15] J. Qu, Z.Q. Ke, A.H. Zuo, Z.H. Rao, Experimental investigation on thermal performance of phase change material coupled with three-dimensional oscillating heat pipe (PCM/3D-OHP) for thermal management application, Int. J. Heat Mass Transf. 129 (2019) 773–782.
- [16] R. Ren, Y. Zhao, Y. Diao, L. Liang, H. Jing, Active air cooling thermal management system based on U-shaped micro heat pipe array for lithium-ion battery, J. Power Sour. 507 (2021), 230314.
- [17] D. Jang, S. Yun, S. Hong, W. Cho, Y. Kim, Performance characteristics of a novel heat pipe-assisted liquid cooling system for the thermal management of lithium-ion batteries, Energy Convers. Manag. 251 (2022), 115001.
- [18] H. Zhou, C. Dai, Y. Liu, X. Fu, Y. Du, Experimental investigation of battery thermal management and safety with heat pipe and immersion phase change liquid, J. Power Sour. 473 (2020), 228545.
- [19] D. Sharma, A. Prabhakar, A review on air cooled and air centric hybrid thermal management techniques for Li-ion battery packs in electric vehicles, J. Energy Storage 41 (2021), 102885.
- [20] A.A. Pesaran, Battery thermal models for hybrid vehicle simulations, J. Power Sour. 110 (2002) 377–382.
- [21] X. Na, H. Kang, T. Wang, Y. Wang, Reverse layered air flow for Li-ion battery thermal management, Appl. Therm. Eng. 143 (2018) 257–262.
- [22] W. Zhuang, Z. Liu, H. Su, G. Chen, An intelligent thermal management system for optimized lithium-ion battery pack, Appl. Therm. Eng. 189 (2021), 116767.
- [23] K. Chen, M. Song, W. Wei, S. Wang, Design of the structure of battery pack in parallel air-cooled battery thermal management system for cooling efficiency improvement, Int. J. Heat Mass Transf. 132 (2019) 309–321.
- [24] K. Kumar, C. Mangesh, Design of cell spacing in lithium-ion battery module for improvement in cooling performance of the battery thermal management system, J. Power Source 481 (2021), 229016.
- [25] Y. Liu, J. Zhang, Self-adapting J-type air-based battery thermal management system via model predictive control, Appl. Energy 263 (2020), 114640.
- [26] X. Li, F. He, G. Zhang, Q. Huang, D. Zhou, Experiment and simulation for pouch battery with silica cooling plates and copper mesh based air cooling thermal management system, Appl. Therm. Eng. 146 (2019) 866–880.
- [27] Y. Liu, J. Zhang, Design a J-type air-based battery thermal management system through surrogate-based optimization, Appl. Energy 252 (2019), 113426.
- [28] F. Zhang, A. Lin, P. Wang, P. Liu, Optimization design of a parallel air-cooled battery thermal management system with spoilers, Appl. Therm. Eng. 182 (2021), 116062.
- [29] M. Wang, S. Teng, H. Xi, Y. Li, Cooling performance optimization of air-cooled battery thermal management system, Appl. Therm. Eng. 195 (2021), 117242.
- [30] J. Hou, X. Wu, K. Chen, Y. Dong, A direct optimization strategy based on field synergy equation for efficient design of battery thermal management system, Int. J. Heat Mass Transf. 184 (2022), 122304.
- [31] J. Chen, X. Zhao, B. Wang, C. Zhang, D. Xuan, Multiobjective optimization of air-cooled battery thermal management system based on heat dissipation model, Ionics 27 (2021) 1307–1322.
- [32] E. Jiaqiang, M. Yue, J.W. Chen, H. Zhu, Y.W. Deng, Y. Zhu, F. Zhang, M. Wen, B. Zhang, S.Y. Kang, Effects of the different air cooling strategies on cooling

- performance of a lithium-ion battery module with baffle, *Appl. Therm. Eng.* 144 (2018) 231–241.
- [33] H. Park, A design of air flow configuration for cooling lithium ion battery in hybrid electric vehicles, *J. Power Source* 239 (2013) 30–36.
- [34] S. Hong, X. Zhang, K. Chen, S. Wang, Design of flow configuration for parallel air-cooled battery thermal management system with secondary vent, *Int. J. Heat Mass Transf.* 116 (2017) 1204–1212.
- [35] S. Shahid, M. Agelin-Chaab, Development and analysis of a technique to improve air-cooling and temperature uniformity in a battery pack for cylindrical batteries, *Therm. Sci. Eng. Progress* 5 (2018) 351–363.
- [36] F. Zhang, M. Yi, P. Wang, C. Liu, Optimization design for improving thermal performance of T-type air-cooled lithium-ion battery pack, *J. Energy Storage* 44 (2021), 103464.
- [37] D. Bernardi, E. Pawlikowski, J. Newman, A general energy balance for battery systems, *J. Electrochem. Soc.* 132 (1985) 5–12.
- [38] K. Chen, Y. Chen, Y. She, M. Song, S. Wang, L. Chen, Construction of effective symmetrical air-cooled system for battery thermal management, *Appl. Therm. Eng.* 166 (2020), 114679.